Journal of Solid State Chemistry **146,** 369–379 (1999)
Article ID jssc.1999.8364, available online at http://www.idealibrary.com on IDEAL®

Structural Study of the Quantum-Spin Chain Compound $(VO)_2P_2O_7$

Z. Hiroi,[1] M. Azuma, Y. Fujishiro, T. Saito, and M. Takano

Institute for Chemical Research, Kyoto University, Uji, Kyoto 611-0011, Japan

F. Izumi

National Institute for Research in Inorganic Materials, 1-1 Namiki, Tsukuba, Ibaraki 305-0044, Japan

T. Kamiyama

Institute of Materials Science, University of Tsukuba, Tennodai, Tsukuba, Ibaraki 305-8573, Japan

and

T. Ikeda

Institute of Applied Physics, University of Tsukuba, Tennodai, Tsukuba, Ibaraki 305-8573, Japan

Received January 20, 1999; in revised form April 30, 1999; accepted May 7, 1999

The crystal structure of the quantum-spin chain compound $(VO)_2P_2O_7$ was studied by electron, X-ray, and neutron diffraction. A polycrystalline sample which clearly exhibited a singlet ground state in magnetic susceptibility measurements was examined. Electron diffraction experiments revealed systematic extinctions which are consistent with an orthorhombic space group $Pca2_1$, in good agreement with previous studies. However, the recent single-crystal X-ray analysis by Nguyen *et al.* concluded that it is monoclinic with space group $P2_1$. This discrepancy may imply that $(VO)_2P_2O_7$ crystallizes in two slightly different structures depending on preparation conditions. The structural parameters of orthorhombic $(VO)_2P_2O_7$ were defined by Rietveld analyses of X-ray and neutron powder diffraction data; $a = 7.73808(7)$ Å, $b = 9.58698(8)$ Å, $c = 16.5895(1)$ Å, and $Z = 8$. Crystallographic disorder was also studied by high-resolution electron microscopy and discussed in terms of positional disorder in the arrangement of the P_2O_7 groups.

INTRODUCTION

Vanadium pyrophosphate $(VO)_2P_2O_7$ has been widely studied by chemists as an efficient catalyst for oxidizing *n*-butane to maleic anhydride. Recently, however, many solid-state physicists have also been interested in this compound because its V^{4+} sublattice was considered an excellent realization of the theoretical spin-ladder model (1, 2). The spin-ladder is a pair of $S = 1/2$ Heisenberg antiferromagnetic (AF) chains coupled antiferromagnetically to form a "ladder-" type lattice (3). Theorists found an unusual many-body, singlet ground state for the spin ladder, where quantum fluctuations prevent ordering of spins even at $T = 0$ K to result in a spin-liquid ground state with an energy gap, called a spin gap, in the excitation spectrum. They also expected to see novel superconductivity when doped with hole carriers, just as seen in high-T_c cuprates. Various magnetic measurements revealed the existence of such a spin gap of about 40 K in $(VO)_2P_2O_7$, which was explained in the framework of the spin-ladder model (1, 4–6).

Contrary to this earlier expectation, however, recent inelastic neutron scattering experiments clarified that $(VO)_2P_2O_7$ can be described as an alternating-spin chain compound, which also should show a similar spin gap, rather than as a spin-ladder compound (7, 8). The source for this confusion is rather complicated superexchange pathways between V^{4+} spins which were difficult to assume straightforwardly by taking only the V^{4+}–O sublattice into consideration. The importance of superexchange interactions through phosphate groups had been pointed out by Beltran and his co-workers in their systematic studies on various oxovanadium(IV) phosphates (9, 10). In fact, according to the inelastic neutron scattering experiments (7), the largest interaction J_1 in $(VO)_2P_2O_7$ was found between VO_5 square pyramids bridged by PO_4 tetrahedra and the second largest interaction J_2 between edge-sharing VO_5

[1] On leave to the Institute for Solid State Physics, University of Tokyo.

0022-4596/99 $30.00

pyramids. These two major interactions form alternating spin chains perpendicular to the "ladder" axis. Thus, $(VO)_2P_2O_7$ is not a spin-ladder compound but still an intriguing compound comprising unusual $S = 1/2$ quantum-spin chains.

One mystery still left to be clarified about $(VO)_2P_2O_7$ is the existence of the second gap of about 70 K which is nearly double the first gap. Garrett *et al.* found this excitation mode in their neutron scattering experiments and suggested that it is associated with the two-magnon bound state. On the other hand, very recent high-field magnetization measurements (11) and NMR studies (12) revealed two independent magnetic subsystems existing in $(VO)_2P_2O_7$: Each system presents a $S = 1/2$ antiferromagnetic alternating chain with a different spin-gap magnitude. It was suggested that $(VO)_2P_2O_7$ comprises two structurally distinguishable V–O chains on the basis of the monoclinic structure given by Nguyen *et al.*

Detailed structural studies are indispensable for understanding the physics of materials. Several crystal structural determinations have already been reported on $(VO)_2P_2O_7$. Initial electron diffraction (ED) and X-ray diffraction (XRD) studies (13, 14) showed orthorhombic symmetry with space group *Pcam* or $Pca2_1$, and the structure was refined by single-crystal X-ray analyses, though *R* factors were not small enough. On the other hand, another single-crystal X-ray analysis by Nguyen *et al.* (15) reached a conclusion that the actual crystal system is monoclinic with space group $P2_1$ ($a = 7.7276(3)$ Å, $b = 16.5885(4)$ Å, $c = 9.5796(5)$ Å, and $\beta = 89.975(3)^\circ$). The fundamental structure determined by them was substantially the same as the previous one. This monoclinic structure has been widely accepted because the refinement ended up with a reasonably small *R* of 3.1%.

One notable structural feature of $(VO)_2P_2O_7$ is crystallographic disorder often detected as streaking effects in its ED and XRD photographs. It has been suggested that incomplete transformation of a precursor $VOHPO_4 \cdot 1/2H_2O$ to $(VO)_2P_2O_7$ which occurs topotactically by dehydration gives rise to the disorder (16). In addition, introduction of stacking faults, which may be relevant to catalytic performance, was also taken into account (17). Nguyen *et al.* claimed that a high-quality crystal with few defects led them to the monoclinic structure (15). The crystal structure of $(VO)_2P_2O_7$ seems to depend on the crystalline quality, synthetic routes, or preparation conditions. We expect that its physical properties can also be affected by these factors. The purpose of this study is to determine the crystal structure of high quality $(VO)_2P_2O_7$ polycrystals which were carefully prepared and proved to exhibit a singlet ground state at low temperature in magnetic susceptibility measurements. The results will enable us to get useful insights on the superexchange pathways that govern the magnetic properties of $(VO)_2P_2O_7$.

EXPERIMENTAL

$(VO)_2P_2O_7$ catalysts have usually been prepared by precipitation from solution or evaporation to dryness and calcination at a moderate temperature (450–550°C). In the present experiments we adopted a simple solid-state reaction between NH_4VO_3 and $NH_4H_2PO_4$ following the method reported by Bordes *et al.* (13). These solid materials were mixed in stoichiometric proportions, pressed into pellets, and calcined successively at 600, 700, and 750°C for 24 h in a CO_2 flow with intermittent grinding and pressing. Finally the sample was heat-treated at 850°C for 24 h in a CO_2 flow where the partial oxygen pressure was about 10^{-6} atm. The color of the polycrystalline sample thus obtained was green. Powder XRD measurements revealed that the diffraction peaks became sharper for samples heat-treated at higher temperatures, suggesting higher crystalline quality. Correspondingly, magnetic susceptibility measurements indicated the smallest Curie components for the sample annealed at 850°C, which means the minimum crystal defects creating free spins at the edge of spin chains. Therefore, further structural refinements were done on the highest temperature annealed sample.

Magnetic susceptibility was measured on a Quantum Design SQUID magnetometer in an applied field of 0.1 T from 2 to 400 K. ED and high-resolution electron microscopy (HREM) observations were carried out on a JEOL-2000EX operating at 200 kV. Specimens for observations were prepared by crushing pellets in acetone and collecting thin fragments on a carbon-coated holey film supported by a copper grid. Simulations for HREM images were done using the MacTempus software.

The XRD data were measured on a Rigaku rotating anode diffractometer with graphite-monochromated Cu$K\alpha$ radiation. Data for Rietveld analyses were collected at room temperature over the 2θ range 10–100° at a 0.02° step for 10 s. Neutron diffraction (ND) data were taken on the high-resolution time-of-flight (TOF) neutron powder diffractometer Vega at the KENS pulsed spallation neutron source. The sample was contained in a cylindrical vanadium can, and the intensity data were collected at room temperature. The coherent scattering lengths used were -0.382 fm, 5.130 fm, and 5.803 fm for V, P, and O, respectively. Intensity data used for the refinement covered a wide *Q* range corresponding to lattice-plane spacings between 0.5 and 5 Å.

RESULTS AND DISCUSSIONS

Magnetic Properties

It is now well established experimentally that $(VO)_2P_2O_7$ has a nonmagnetic singlet ground state. Thus, the spin susceptibility should decrease exponentially at low temperature and vanish at $T = 0$ K. The magnetic susceptibility

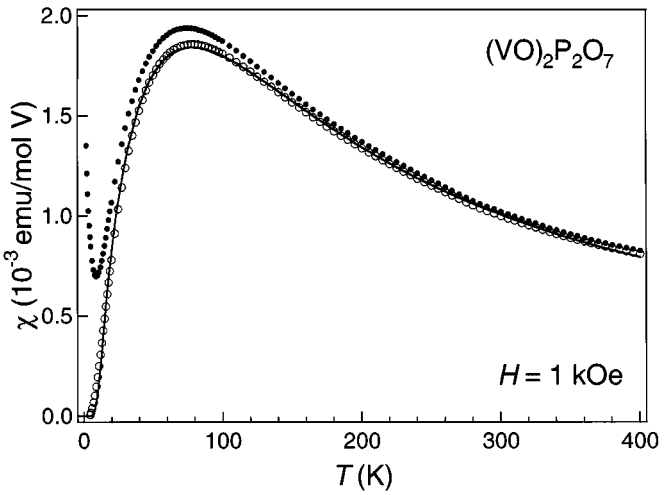

FIG. 1. Temperature dependence of magnetic susceptibility χ for $(VO)_2P_2O_7$. The data (filled circles) were measured with increasing temperature from 2 to 400 K in a magnetic field of 1 kOe. The open circles show the spin susceptibility obtained after subtraction of the free spin contribution (1.7%) at low temperature. The solid line is a fit to the spin susceptibility data, assuming an alternating-spin chain model with $J_1/k_B = 130.9$ (5) K, $\alpha = J_2/J_1 = 0.782(2)$, and $g = 2.021(2)$.

χ measured for our $(VO)_2P_2O_7$ powders showed a broad maximum around 70 K and decreased rapidly with decreasing temperature, followed by an upturn below 10 K, as shown in Fig. 1. The broad peak suggests that short-range AF ordering occurs. From an inverse χ versus T plot below 10 K, the density of almost free spins with a Curie–Weiss temperature of -3 K was estimated to be 1.7%, which is as small as previously reported (1). These free spins may come from the edge state of alternating chains occasionally produced by lattice imperfections, as generally observed in one-dimensional spin compounds. Therefore, the present sample is considered to have good crystalline quality similar to those previously used for physical characterization.

The spin susceptibility was obtained by subtracting the above defect contribution from the observed $\chi(T)$ data and plotted in Fig. 1. In the framework of the $S = 1/2$ Heisenberg AF alternating chain model (5, 18), we could fit the data with three variable parameters; $J_1/k_B = 130.9(5)$ K, $\alpha = J_2/J_1 = 0.782(2)$, and $g = 2.0021(2)$. J_1 is a larger superexchange interaction along the c axis probably through PO_4 groups, and J_2 is a smaller one between the nearest neighbor V^{4+} spins. The g-factor obtained was close to the value ($g = 1.98$) determined by ESR measurements (19). The J_1 and α determined in the present study are in good agreement with those reported in the previous studies, i.e., $J_1/k_B = 131.3$ K and $\alpha = 0.7$ by Johnston (1), and $J_1/k_B = 128.9$ K and $a = 0.722$ by Barnes (5). Our α value seems slightly larger than the previous ones, which may reflect small differences in bond lengths or angles in the V–O lattice. We note here that our $(VO)_2P_2O_7$ sample has well been characterized as representing $S = 1/2$ alternating chains, though small amount of crystal defects may exist.

Electron Diffraction and Microscopy

Electron beams are powerful probes to determine the symmetry of a crystal, as well as to detect local structural deviations from an average structure. As mentioned above, the space group of $(VO)_2P_2O_7$ was first determined to be $Pcam$ or $Pca2_1$, but was concluded to be $P2_1$ in the latest single-crystal XRD analysis. Here we examined about 30 fragments (tiny single crystals) in an electron microscope and recorded various cross sections of the reciprocal lattice to determine unequivocally the space group of our $(VO)_2P_2O_7$.

ED patterns along the main zone axes are reproduced in Fig. 2, where diffraction spots are indexed with an orthorhombic cell of $a = 7.7$ Å, $b = 9.6$ Å, and $c = 16.6$ Å. Each pattern exhibits a simple rectangular mesh, implying a primitive Bravais lattice. Reflection conditions apparently observed are $l =$ even for $0kl$ reflections (Fig. 2a) and $h =$ even for $h0l$ reflections (b), revealing the existence of c-glide and a-glide planes, respectively. No extinctions are seen for $hk0$ reflections (c). Additional conditions observed are $h =$ even for $h00$ and $l =$ even for $00l$. The unexpected appearance of $00l$ reflections with $l =$ odd in Fig. 2b and the $h00$ reflections with $h =$ odd in Fig. 2c is due to double diffraction, as examined in tilting experiments. Possible space groups consistent with the observed reflection conditions are only orthorhombic $Pcam$ or $Pca2_1$, in perfect agreement with previous results except those of Nguyen *et al.* Though ED experiments cannot detect a small monoclinic distortion, the present symmetry restriction is strong enough to exclude the possibility of less symmetrical space groups. Moreover, no traces of crystal twinning were observed in the present microscopy observations: Twinning often appears for a crystal with a small monoclinic distortion like CuO. We imagine that the single crystal analyzed by Nguyen *et al.* has crystal structures substantially different from ours because they observed those forbidden reflections in the X-ray measurements and used them for the structural determination. It is plausible that $(VO)_2P_2O_7$ exhibits at least two slightly different crystal structures depending on the preparation conditions. Their single crystal was grown from a high-temperature melt by slow cooling under appropriate control of oxygen fugacity, whereas our polycrystalline sample was prepared at a lower temperature by solid-state reaction. We have not seen clear violations of the extinctions in most of fragments examined, although ED is generally more sensitive for weak reflections due to dynamical effects than XRD. In small portion of fragments, however, we found diffuse streaking due to crystallographic disorder, as will be described later. It should be noted here

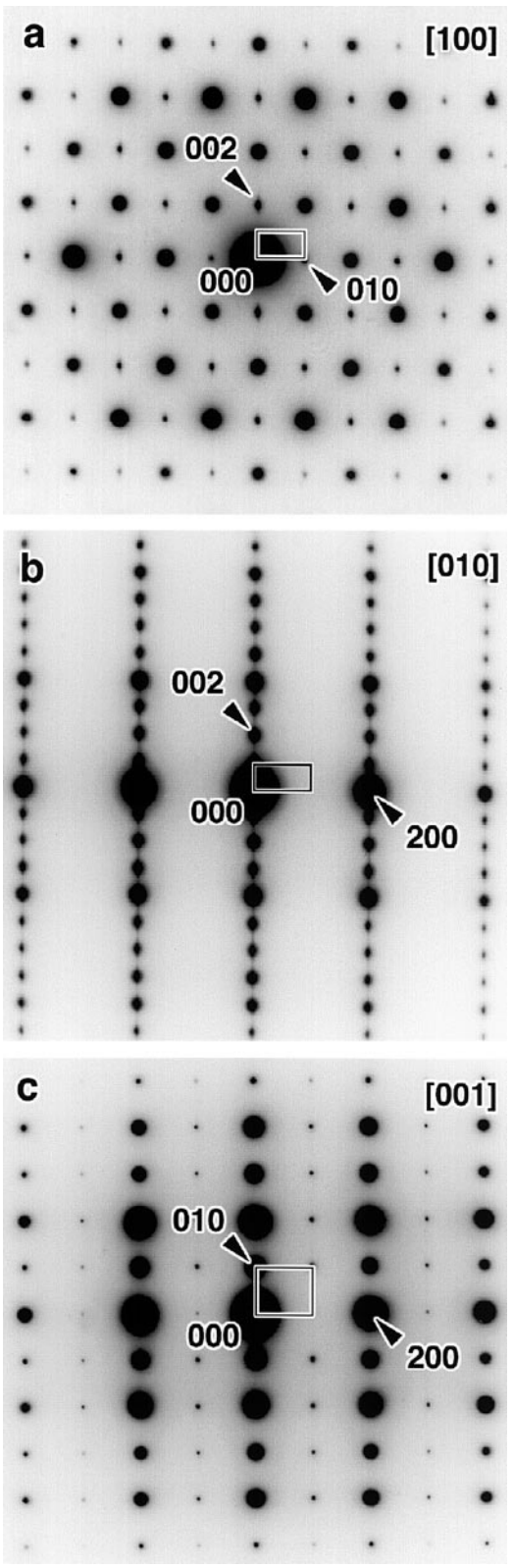

FIG. 2. Electron diffraction patterns of main zone axes for $(VO)_2P_2O_7$. Systematic extinctions are apparent in the [100] (a) and [010] (b) zone axes, whereas they are missing in the [001] zone axis (c). Projection of the unit cell in the reciprocal space is shown with the rectangle.

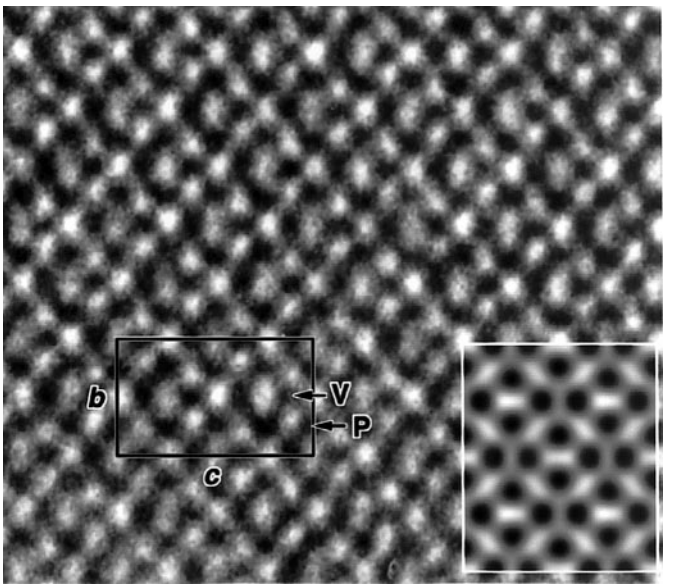

FIG. 3. High-resolution electron microscopy image taken with the incident electron beam parallel to the [100] direction. A computer-simulated image is shown at the right bottom corner.

that the introduction of disorder apparently violates the extinctions and thus tends to mislead us into accepting lower crystal symmetries.

The crystal structure of $(VO)_2P_2O_7$ was approximately visualized by HREM. Figure 3 reproduces a typical HREM image taken with the incident electron beam parallel to the *a* axis. The atomic columns of V and P are well resolved as dark dots, and their arrangement is certainly consistent with the previous structural model projected along the *a* axis. The repeat distance of the patterns along the *c* axis is half the *c* length because of the existence of a *c*-glide with reflection across the paper plane. Fairly good agreement is seen between observed and calculated images on the basis of the Rietveld analyses described below.

Structural Refinements

Structural refinements were carried out by repeating Rietveld analyses of XRD and ND data alternately. The reason is that vanadium atoms are almost "transparent" to neutrons, whereas oxygen atoms have relatively small atomic scattering factors for X-rays. In each refinement with RIETAN (20), structural parameters determined in the last refinement were used as initial ones, and this feedback process was repeated several times. In the final process, the atomic coordinates and the thermal parameters of all of the atoms were first determined by using the ND data, and then only those of V atoms were refined, keeping those of P and O atoms intact. Taking account of limited information in the powder patterns and the many structural parameters to

be refined, the following nonlinear constraints were imposed in the Rietveld analyses: The bond lengths between V atoms and the nearest neighbor O atoms should be within the limits of 1.58 Å to 1.62 Å, and bond lengths between P and O atoms between 1.53 Å and 1.57 Å. Unusually large anisotropic profile broadening was observed, particularly in the low-angle region of the XRD data and in the low-Q region in the ND data, which made it difficult to fit the profile function used in RIETAN to the observed profiles. Thus, a new technique called partial profile relaxation (21) was applied, which enabled us to fit the profiles of 14 (18) selected reflections in the XRD (ND) data independently of the overall profile function for the other reflections. The resulting fit was dramatically improved by this method.

The basic crystal structure of $(VO)_2P_2O_7$ has been well established in previous studies (13, 15). The purpose of our study was to refine the structural parameters of our sample showing a singlet ground state with minimum magnetic defects. We assumed the noncentrosymmetrical space group $Pca2_1$ on the basis of the ED results because the other possible space group $Pcam$ was found to be unacceptable to reproduce the basic structure. The key to the refinements was to build a good starting model as close to the "true" structure as possible because of limited structural information obtainable from the powder diffraction data. Thus, we used the most reliable data of Nguyen *et al.* (15). We noticed that combination of an appropriate pair of atoms at the 2*a* sites in their $P2_1$ model could create one atom at the 4*a* site in $Pca2_1$, probably because of a small deviation from orthorhombic symmetry in their crystal. For example, the presence of an equivalent position $(\bar{x} + 1/2,\ y,\ z + 1/2)$ in $Pca2_1$ leads to the copying of V1 (0.2973, 0.4912, 0.0958) in the $P2_1$ model at V1′ (0.2027, 0.4912, 0.5958) which is nearly identical to V2 (0.2039, 0.4909, 0.5960) in the $P2_1$ model. In this way, a starting $Pca2_1$ model was built and refined by a series of alternating Rietveld refinements of the XRD and ND data. The resulting structural parameters and their estimated standard deviations are listed in Table 1. Figure 4 illustrates the Rietveld refinement patterns for the XRD and ND data, showing excellent fits between the observed and calculated patterns. No forbidden reflections for space group $Pca2_1$ were detected in either pattern. Lattice constants refined by ND were $a = 7.73808(7)$ Å, $b = 9.58698(8)$ Å, and $c = 16.5895(1)$ Å. R factors were $R_{wp} = 3.47\%$, $R_e = 3.60\%$, $R_p = 2.66\%$, $R_B = 1.15\%$, and $R_F = 1.06\%$ for ND and $R_{wp} = 7.89\%$, $R_e = 8.29\%$, $R_p = 5.97\%$, $R_B = 1.85\%$, and $R_F = 1.09\%$ for XRD. The goodness-of-fit index R_{wp}/R_e was 0.96 and 0.95, and the Durbin–Watson statics d were 1.26 and 0.54, respectively.

The structure determined in the present study is essentially the same as that found in previous studies, as shown in Fig. 5. The metal–oxygen bond lengths l for V and P are listed in Table 2. The bond valence sums (BVS) were calculated with $\mathrm{BVS} = \sum \exp((r_0 - r_i)/B)$ where $B = 0.37$ Å, r_i is the bond length, and r_0 is 1.784 Å for the V^{4+}–O^{2-} bond and 1.617 Å for the P^{5+}–O^{2-} bond (22). Bond valence sums at each site gave reasonable values for V^{4+} and P^{5+}. The vanadium atoms square-pyramidally coordinated to five oxygen atoms with one short bond ($l \sim 1.6$ Å) and four nearly equatorial bonds ($l \sim 2$ Å), but also weakly coordinated along the a axis to the apex oxygen belonging to the neighboring VO_5 pyramid with a long bond length of about 2.3 Å. Two of the VO_5 square pyramids are tightly connected by sharing their edges along the c axis with each apex oxygen above or below the basal plane. These VO_5 pairs are linked by pyrophosphate groups to yield a three-dimensional skeleton. A major difference between the $Pca2_1$ and $P2_1$ models is found in whether or not two nearby V atoms aligned along the a axis are symmetrically related.

A recent inelastic neutron diffraction study (7) has revealed that major magnetic interaction occurs along the c axis. A surprisingly large AF superexchange interaction J_1 through pyrophosphate groups was suggested, and the second largest AF interaction J_2 ($J_2/J_1 \sim 0.8$) was found between V^{4+} spins in the pair of VO_5 pyramids. The

TABLE 1
Fractional Atomic Coordinates and Atomic Displacement Parameters for $(VO)_2P_2O_7$

Atom	Wyckoff position	x	y	z	B_{eq} (Å^2)
V1	4*a*	0.212(5)	0.492(12)	0.598(6)	1.13
V2	4*a*	0.197(4)	0.517(10)	0.907(7)	1.13
V3	4*a*	0.214(5)	− 0.002(13)	0.841(6)	1.13
V4	4*a*	0.206(5)	− 0.004(13)	0.153(6)	1.13
P1	4*a*	0.200(2)	0.703(2)	0.755(2)	0.60
P2	4*a*	0.194(3)	0.290(2)	0.257(2)	1.30
P3	4*a*	0.198(2)	0.796(2)	0.500(3)	0.51
P4	4*a*	0.203(3)	0.207(2)	0.000	1.25
O1	4*a*	0.013(3)	0.463(1)	0.590(2)	0.55
O2	4*a*	− 0.005(3)	0.534(1)	0.910(2)	1.74
O3	4*a*	− 0.005(4)	− 0.012(1)	0.341(2)	1.01
O4	4*a*	− 0.003(4)	0.007(1)	0.161(2)	1.20
O5	4*a*	0.005(3)	0.821(1)	0.502(2)	1.87
O6	4*a*	− 0.006(3)	0.289(1)	0.286(1)	1.60
O7	4*a*	0.218(2)	0.633(2)	0.500(2)	1.30
O8	4*a*	0.221(2)	0.363(2)	− 0.002(2)	0.51
O9	4*a*	0.248(3)	0.130(2)	0.249(2)	0.64
O10	4*a*	0.250(3)	0.859(2)	0.251(2)	0.28
O11	4*a*	0.210(2)	0.644(2)	0.675(2)	0.57
O12	4*a*	0.212(3)	0.359(2)	0.175(2)	0.88
O13	4*a*	0.216(3)	0.629(2)	0.325(2)	1.92
O14	4*a*	0.207(2)	0.358(2)	0.823(2)	0.74
O15	4*a*	0.231(3)	0.137(2)	0.573(2)	0.92
O16	4*a*	0.228(4)	0.858(2)	0.076(2)	2.10
O17	4*a*	0.233(3)	0.141(2)	0.425(2)	0.92
O18	4*a*	0.219(3)	0.846(2)	0.926(2)	1.20

Note. Space group $Pca2_1$ (No. 29); $a = 7.73808(7)$ Å, $b = 9.58698(8)$ Å, and $c = 16.5895(1)$ Å; $Z = 8$. $B_{eq} = (8\pi^2/3)\sum_i\sum_j U_{ij}a_i^*a_j^*a_ia_j$.

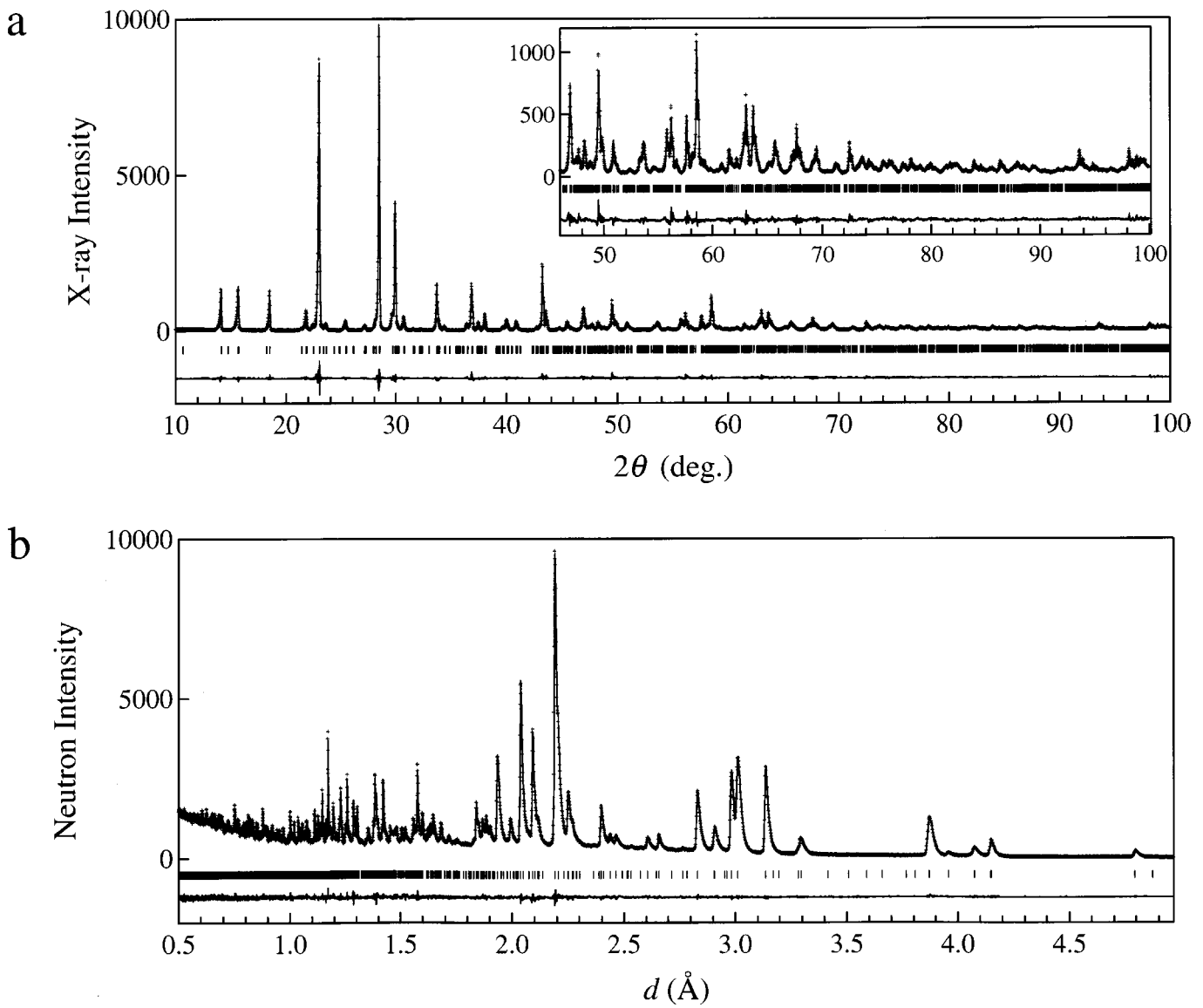

FIG. 4. Rietveld-refinement patterns for (a) XRD and (b) ND data. Observed diffraction intensities are represented by plus (+) marks, and the calculated patterns by the solid lines. Differences between the observed and calculated intensities are given near the bottom. Short vertical marks indicate the position of allowed Bragg reflections.

coupling along the *a* axis, which was believed to be large in earlier studies, is weakly ferromagnetic, and that along the *b* axis is almost negligible. Then, vanadyl chains running along the *c* axis should represent $S = 1/2$ alternating chain with J_1 and J_2 exhibiting a spin gap.

It is interesting to note that there are two crystallographically different vanadyl chains in the unit cell: V1–V2 and V3–V4 chains (Fig. 5). The two chains are apparently distinguished from each other, when viewed along the *b* axis, as compared in Figs. 5b and 5c. The V1–V2 chain which consists of edge-sharing V1–V2–O pyramids linked by P1–O and P2–O tetrahedra winds along the *c* axis owing to the tilting of the PO_4 tetrahedra. In contrast, the V3–V4 chain is rather on the straight with untilted P3–O and P4–O tetrahedra. J_1 and J_2 may be slightly different between the two chains because they must depend on bond lengths and bond angles, as well as deformation of the V–O pyramids. It is expected that the magnetic properties of the two chains are different. The result is consistent with the recent high-field magnetization measurements and NMR studies (11, 12). It was suggested that there are two independent alternating chains with different spin gaps and exchange couplings, which are summarized in Table 3 together with some related structural parameters obtained in the present

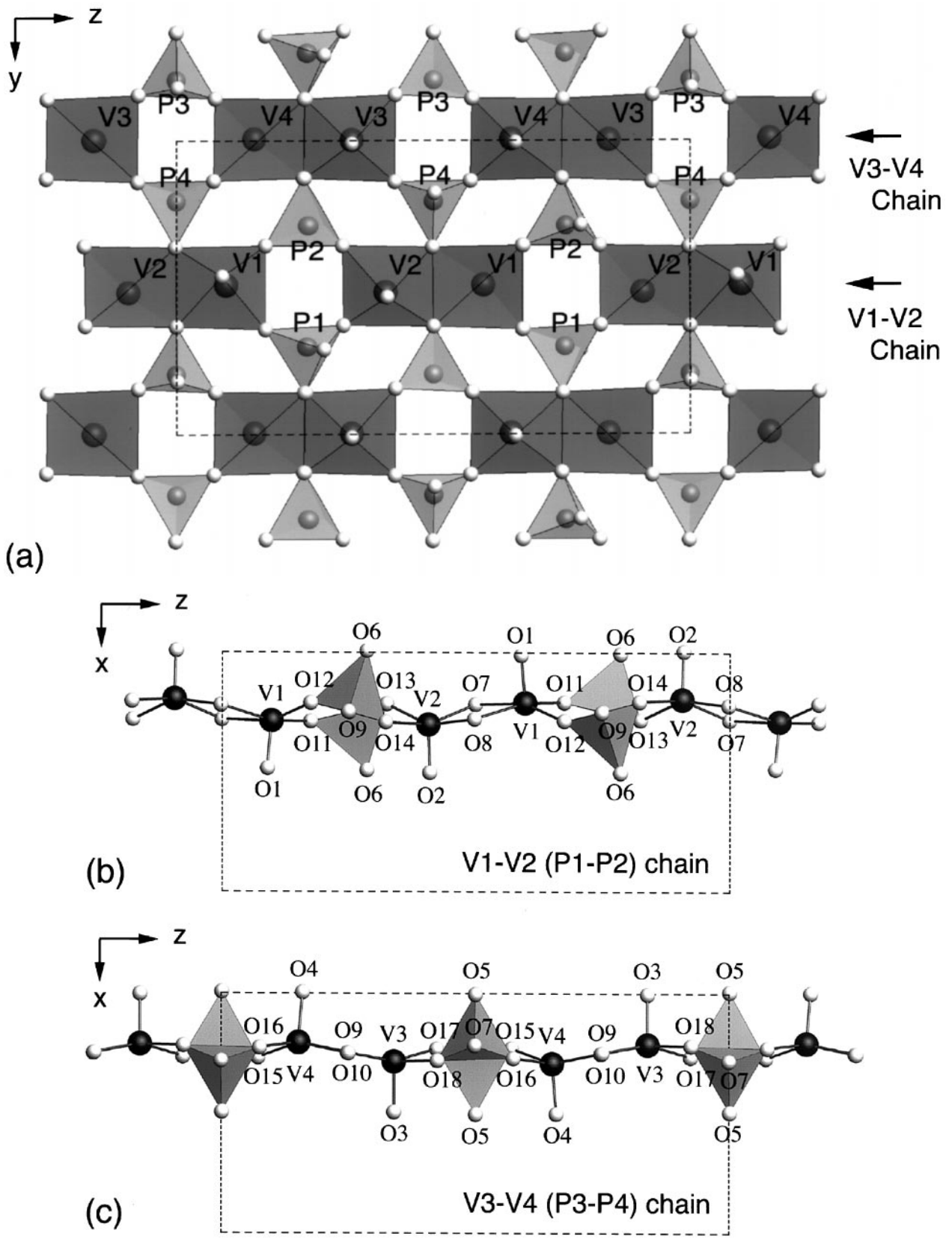

FIG. 5. (a) Two V–O chains each representing $S = 1/2$ Heisenberg antiferromagnetic alternating chains in $(VO)_2P_2O_7$. (b and c) The two crystallographically different chains viewed along the *b* axis. Large, medium, and small balls represent V, P, and O atoms, respectively.

TABLE 2
Selected Bond Lengths (l) and Bond Valence Sums (BVS) in $(VO)_2P_2O_7$

Atom		l (Å)	BVS	Atom		l (Å)	BVS
V1	O1	1.57(3)	4.17	P1	O18	1.47(3)	5.30
	O1′	2.37(3)			O16	1.51(3)	
	O12	1.90(10)			O5	1.51(3)	
	O11	1.94(12)			O7	1.57(2)	
	O7	2.12(10)		P2	O17	1.48(3)	5.20
	O8	2.13(12)			O15	1.48(3)	
V2	O2	1.57(3)	4.23		O8	1.51(2)	
	O2′	2.36(3)			O5	1.64(3)	
	O13	1.86(9)		P3	O11	1.44(3)	5.23
	O7	2.01(12)			O13	1.52(3)	
	O14	2.06(12)			O10	1.54(2)	
	O8	2.12(9)			O6	1.59(3)	
V3	O3	1.62(4)	3.98	P4	O14	1.49(3)	4.76
	O3′	2.25(4)			O12	1.51(3)	
	O17	2.01(11)			O9	1.60(2)	
	O9	2.01(11)			O6	1.62(3)	
	O10	2.01(11)					
	O18	2.03(11)					
V4	O4	1.63(3)	4.12				
	O4′	2.26(4)					
	O16	1.86(12)					
	O15	1.95(11)					
	O9	2.06(11)					
	O10	2.12(11)					

study. Our V1–V2 (V3–V4) chains correspond to the V1–V2–V3–V4 (V5–V6–V7–V8) chains in the monoclinic structure. Kikuchi *et al.* ascribed the origin of the differences in spin gap to the small differences in the V–V distance on the basis of the monoclinic model (12). Generally, exchange interactions decrease sensitively with increasing interatomic distances. The V–(O)–V distances (related to J_2) in the edge-sharing pyramids are 3.22 Å and 3.20 Å for the V1–V2–V3–V4 and V5–V6–V7–V8 chains, respectively, and the V–(PO_4)–V distances (J_1) via PO_4 units are 5.14 Å and 5.16 Å in the monoclinic structural model. This indicates larger J_1 and smaller J_2 in the former chains, giving a larger J_2/J_1 ratio and a larger spin gap, which can explain qualitatively the physical experimental results. However, we have to be delicate in discussing the magnitude of J with such a small difference in the V–V distance (0.02 Å), particularly for the long V–(PO_4)–V distances. In the present orthorhombic model, the differences in the V–(O)–V and V–(PO_4)–V distances between the two chains were found to be much larger, 0.08 Å and 0.05 Å, respectively. Therefore, it is reasonably concluded that the V1–V2 chains have a larger alternation than the V3–V4 chains. Further quantitative analyses of the magnitude of J require detailed evaluation of the overlap integral of orbitals, taking account of the deformation of V–O pyramids, as well as the contribution of PO_4 units.

Crystal Defects in $(VO)_2P_2O_7$

Crystallographic disorder in $(VO)_2P_2O_7$ has been extensively studied in relation to the dehydration process of the precursor. Here we describe the disorder found by electron microscopy in our polycrystalline sample and briefly discuss its origin. Though we tried to optimize the preparation conditions to remove defects completely, magnetically free V spins of 1.7% were found in the susceptibility measurements which may be attributed to occasional cutting of the spin chains. Careful examination by an electron microscope revealed that most of the fragments of a typical size of 1 μm were defect-free, but some exhibited characteristic streaking in the ED patterns, such as shown in Fig. 6. The existence of additional diffuse intensity becomes clear, if one compares Fig. 6a with Fig. 2b taken in the same zone axis, [010]: Weak diffuse lines appear halfway between the spot rows. Tilting experiments, such as shown in Figs. 6b and 6c, evidenced that diffuse scattering intensity extended two-dimensionally perpendicular to the a^* axis. A small intensity modulation was detected in the tilting series, stronger in the $[01\bar{1}]$ zone axis than the [010] zone axis, which was partly due to dynamical effects. The corresponding HREM image taken with the $[01\bar{1}]$ ED pattern of Fig. 6c is shown in Fig. 7. Irregular phase contrasts were seen overlapped on the two orthogonal sets of lattice fringes, (100) and (011), in the whole area in the aperture used. As typically marked in the figure, vertical, bright dot rows about 10 nm long along the a axis appear from place to place. It is obvious from this HREM image, as well as from the fact that streaking extends two-dimensionally, that the entity of the defect is the occurrence of short strings of atomic disorder running along the [100] direction without structural coherence perpendicular to the [100] direction.

TABLE 3
Selected Distances and Angles for the V1–V2 and V3–V4 Chains in Orthorhombic $(VO)_2P_2O_7$ and the Magnitude of Spin Gap (Δ) and Exchange Interactions (J_1 and J_2) reported by Kikuchi *et al.* (12)

	V1–V2 Chain	V3–V4 Chain
Distance (Å)		
V–(O)–V (J_2)	3.26	3.18
V–(PO_4)–V (J_1)	5.13	5.18
Angle (°)		
V1–O7–V2	104.1	
V1–O8–V2	99.9	
V3–O9–V4		102.5
V3–O10–V4		100.4
Δ(K)	68	35
J_1/k_B(K)	136	124
J_2/k_B(K)	92	103

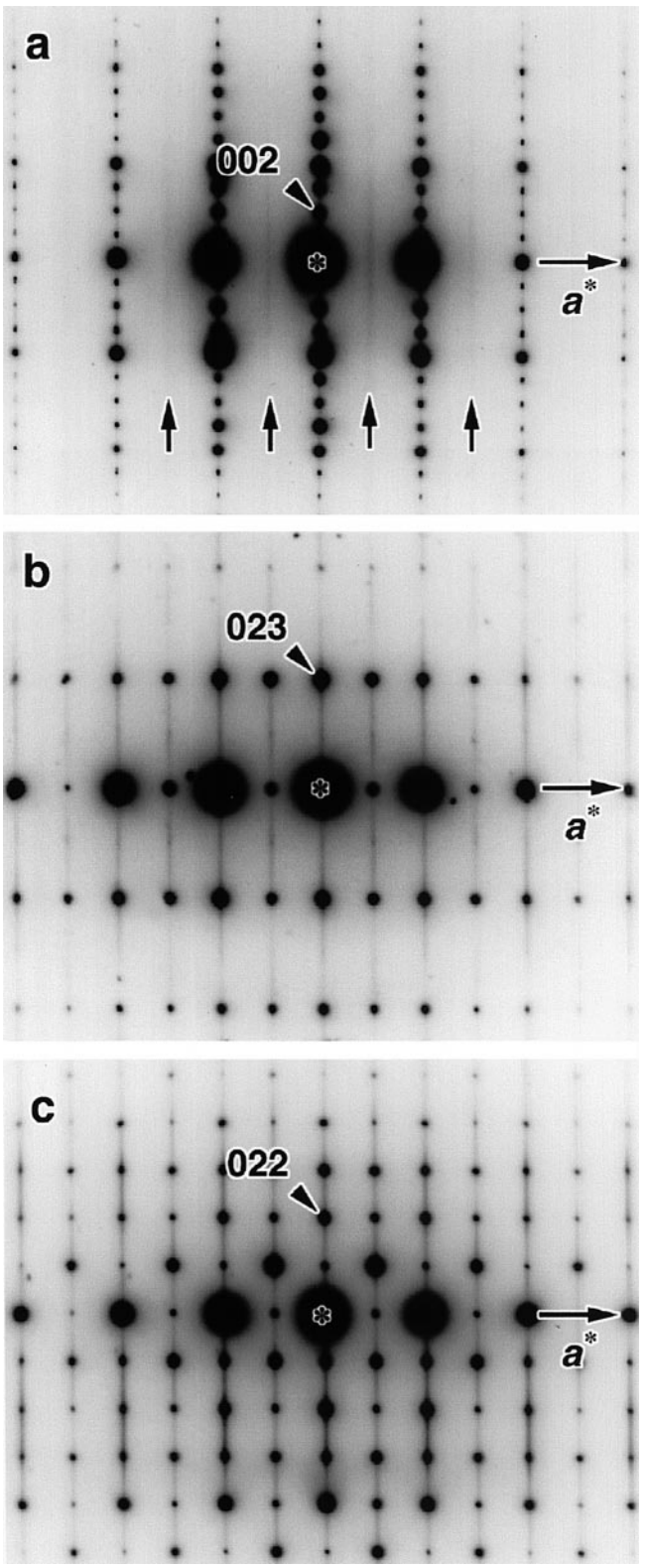

FIG. 6. ED patterns taken from fragments containing crystal defects. Diffuse lines due to disorder are marked with arrows in the [010] zone axis (a). (b) and (c) were recorded in a series of tilting experiments on the same fragment. Note that the streaking always exists perpendicular to the a^* axis.

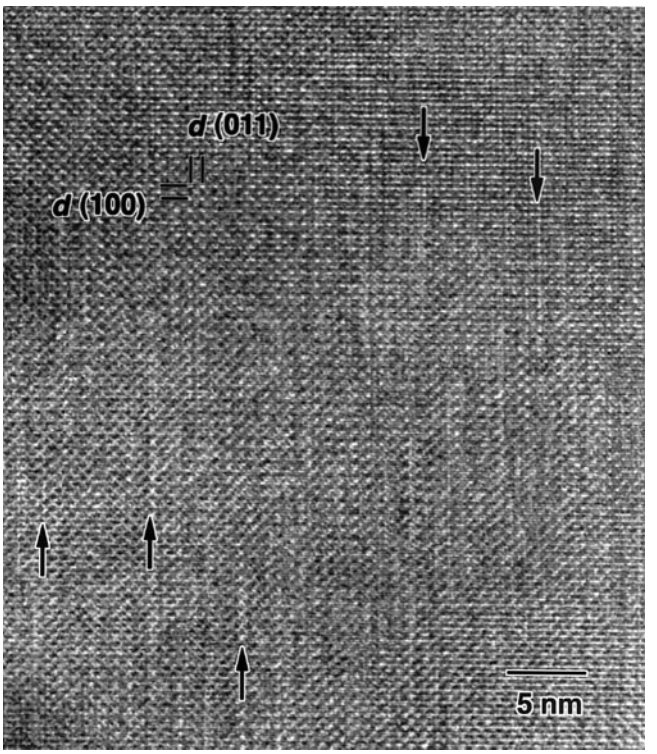

FIG. 7. HREM image taken with the ED pattern shown in Fig. 6c. Crystal defects responsible for the streaking observed in the ED pattern are clearly seen as vertical, bright dot rows as typically marked with arrows.

It is not easy to extract meaningful information about the origin of the defects in $(VO)_2P_2O_7$ from our Rietveld analyses. However, we noticed some oxygen sites in the P_2O_7 groups with unusually large atomic displacement parameters. Particularly noted is the O5 site that is shared by two opposing PO_4 tetrahedra in the P_2O_7 group. Nguyen *et al.* also reported unusually large atomic displacement parameters for the O9 and O10 sites in their model which in fact correspond to the O5 site in our analyses, though they did not make any comments on this important fact. We believe that certain disorder in the O5 site can give a plausible explanation for the characteristic defects in $(VO)_2P_2O_7$. One possible scenario is as follows. A local jump of O5 oxygens by $a/2$ above or below to vacancies between the adjacent P_2O_7 groups may easily occur because it just changes the position of P_2O_7 groups to result in the phase shift of P_2O_7 rows along the a axis and maintains the V–O sublattice almost intact (Fig. 8). It is noted that, if such a jump occurs at a certain P_2O_7 group, all of the O5 oxygens in the same P_2O_7 column along the a axis should move synchronously so as not to break any P_2O_7 groups. This must give rise to linear defects extending along the a axis.

Torardi *et al.* studied the transformation of $VOHPO_4 \cdot 1/2H_2O$ to $(VO)_2P_2O_7$ and suggested that the hydrogen

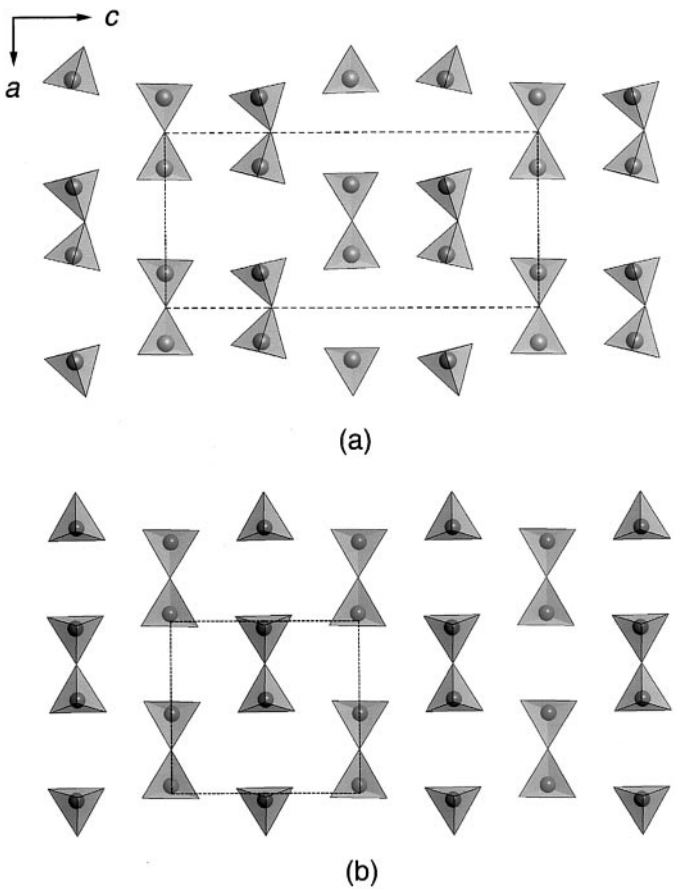

FIG. 8. Schematic illustrations of two arrangements of P_2O_7 groups for the ambient-pressure form (a) and the high-pressure form (b). The high-pressure type arrangement can be mixed into the ambient-pressure form as a defect, which may give a reasonable explanation for the observed disorder in $(VO)_2P_2O_7$.

phosphate groups condense into pyrophosphate moieties through an inversion of the phosphorous centers (16). They claimed that disorder produced in this inversion process, which may be similar, as we have discussed, was responsible for the streaking. We believe that the positional disorder of P_2O_7 groups mentioned above is more general and intrinsic for the crystal structure of $(VO)_2P_2O_7$ because our sample was prepared directly through the solid-state reaction of NH_4VO_3 and $NH_4H_2PO_4$ at high temperature.

Very recently, Azuma *et al.* found an interesting structural phase transition of $(VO)_2P_2O_7$ under high pressure (23). When the ambient-pressure phase was annealed at 2 GPa and 700°C and then quenched, a new high-pressure form was obtained. The crystal structure of the polycrystals thus obtained was analyzed by ED, XRD, and ND, as in the present study, and found to be very similar to that of the ambient-pressure form. The c axis dimension of the orthorhombic unit cell of the former is nearly half that of the latter, and the other dimensions are almost the same; $a =$ 7.5801(2) Å, $b = 9.5458(3)$ Å, $c = 8.3629(3)$ Å, and $Z = 4$ for the high-pressure form. The space group was determined to be *Pnab* (No. 60). A substantial difference is found in the arrangement of P_2O_7 groups, as schematically depicted in Fig. 8. In the ambient-pressure form a pair of P_2O_7 columns along the a axis are in the same phase, and a phase shift occurs at the next pair of columns. In contrast, the same phase shift occurs in every P_2O_7 column in the high-pressure form. This fact implies that there are at least two thermodynamically stable structures for $(VO)_2P_2O_7$ in the arrangement of P_2O_7 groups. It is presumable that the two arrangements appear mixed at certain conditions or that one is contained as a defect in the other. This is in fact what we expected for the defect in the ambient-pressure form of $(VO)_2P_2O_7$. The Rietveld analyses of the high-pressure form also showed an exceptionally large thermal parameter for the central oxygen site of P_2O_7 groups.

CONCLUSIONS

The crystal structure of the quantum-spin chain compound $(VO)_2P_2O_7$ was reexamined by electron, X-ray, and neutron diffraction, using a polycrystalline sample that clearly exhibited a singlet ground state in magnetic susceptibility measurements. An orthorhombic structural model of space group $Pca2_1$ was refined by Rietveld analyses. It is suggested that $(VO)_2P_2O_7$ can crystallize both in monoclinic and orthorhombic structures depending on the preparation conditions. The key to understanding the characteristic crystallographic disorder was suggested to be positional disorder in the arrangement of P_2O_7 groups.

ACKNOWLEDGMENTS

This work was supported in part by CREST (Core Research for Evolutional Science and Technology) of the Japan Science and Technology Corporation.

REFERENCES

1. D. C. Johnston, J. W. Johnson, D. P. Goshorn, and A. J. Jacobson, *Phys. Rev. B* **35,** 219 (1987).
2. E. Dagotto, J. Riera, and D. Scalapino, *Phys. Rev. B* **45,** 5744 (1992).
3. E. Dagotto and T. M. Rice, *Science* **271,** 618 (1996).
4. R. S. Eccleston, T. Barnes, J. Brody, and J. W. Johnson, *Phys. Rev. Lett.* **73,** 2626 (1994).
5. T. Barnes and J. Riera, *Phys. Rev. B* **50,** 6817 (1994).
6. J. Kikuchi, T. Yamauchi, and Y. Ueda, *J. Phys. Soc. Jpn* **66,** 1622 (1997).
7. A. W. Garrett, S. E. Nagler, D. A. Tennant, B. C. Sales, and T. Barnes, *Phys. Rev. Lett.* **79,** 745 (1997).
8. T. Barnes, J. Riera, and D. A. Tennant, *Phys. Rev. B* **59,** 11384 (1999).
9. D. Beltran-Porter, P. Amoros, R. Ibanez, E. Martinez, A. Beltran-Porter, A. L. Bail, G. Ferey, and G. Villeneuve, *Solid State Ionics* **32/33,** 57 (1989).
10. P. Amoros, A. Beltran, and D. Beltran, *J. Alloys Compd.* **188,** 123 (1992).

11. T. Yamauchi, Y. Narumi, J. Kikuchi, Y. Ueda, K. Tatani, T. C. Kobayashi, K. Kindo, and K. Motoya, submitted for publication.
12. J. Kikuchi, K. Motoya, T. Yamauchi, and Y. Ueda, *J. Phys. Soc. Jpn.*, in press.
13. E. Bordes and P. Courtine, *J. Catalysis* **57,** 236 (1979).
14. Y. E. Gorbunova and S. A. Linde, *Sov. Phys. Dokl.* **24,** 138 (1979).
15. P. T. Nguyen, R. D. Hoffman, and A. W. Sleight, *Mater. Res. Bull.* **30,** 1055 (1995).
16. C. C. Torardi, Z. G. Li, H. S. Horowitz, W. Liang, and M.-H. Whangbo, *J. Solid State Chem.* **119,** 349 (1995).
17. P. T. Nguyen, A. W. Sleight, N. Roberts, and W. W. Warren, *J. Solid State Chem.* **122,** 259 (1996).
18. J. C. Bonner and H. W. J. Blöte, *Phys. Rev. B* **25,** 6959 (1982).
19. H. Schwenk, M. Sieling, D. König, W. Palme, S. A. Zvyagin, B. Lüthi, and R. S. Eccleston, *Solid State Commun.* **100,** 381 (1996).
20. F. Izumi, in "The Rietveld Method" (R. A. Young, Ed.), p. 236. Oxford University Press, Oxford, 1993.
21. T. Ohta, F. Izumi, K. Oikawa, and T. Kamiyama, *Physica B* **234-236,** 1093 (1997).
22. I. D. Brown and D. Altermatt, *Acta Crystallogr. B* **41,** 244 (1985).
23. M. Azuma, T. Saito, Y. Fujishiro, Z. Hiroi, M. Takano, F. Izumi, T. Kamiyama, T. Ikeda, Y. Narumi, and K. Kindo, *Phys. Rev. B*, in press.